Applied Catalysis B: Environmental 89 (2009) 602–612

Contents lists available at ScienceDirect

Applied Catalysis B: Environmental

journal homepage: www.elsevier.com/locate/apcatb

Fast adsorptive and photocatalytic purification of air from acetone and dimethyl methylphosphonate by TiO_2 aerosol

A.S. Besov, A.V. Vorontsov *, V.N. Parmon

Boreskov Institute of Catalysis and Novosibirsk State University, Novosibirsk 630090, Russian Federation

ARTICLE INFO

Article history:
Received 6 November 2008
Received in revised form 20 January 2009
Accepted 24 January 2009
Available online 3 February 2009

Keywords:
Atmospheric chemistry
CWA
Photocatalysis
Titanium dioxide
Titania
Decontamination
Anti-terrorism
Water concentration
Gas phase
Static
Nanoparticles
Phosphoric acid
Troposphere

ABSTRACT

A high concentration (1.5×10^6 cm^{-3}) TiO_2 aerosol of the average particle size 0.5 μm was generated by a sonic method inside 0.1 m^3 Plexiglas chamber and applied for the adsorptive and adsorptive-photocatalytic purification of air from vapors of acetone and chemical agents' model dimethyl methylphosphonate (DMMP). The adsorptive capture of acetone over the TiO_2 aerosol results in establishing equilibrium adsorption state and is limited by the rate of the aerosol admission into the chamber. A model derived from the Langmuir isotherm describes well the acetone concentration vs. aerosol mass curve and allows obtaining the adsorption constant and monolayer coverage of acetone in a 10 min experiment. The UV irradiation of TiO_2 aerosol accelerates dramatically the purification from acetone at the high relative humidity (RH) of the air. Increased RH of air decreases the rate of the acetone adsorption but has a little positive effect on the rate of photocatalytic oxidation of acetone over aerosol particles. The DMMP adsorption over TiO_2 aerosol is accompanied by the immediate ($\tau < 10$ s) and irreversible hydrolysis of DMMP with the formation of gas phase methanol and adsorbed methyl methylphosphonic acid. The irreversible reactive adsorption results in the very fast air purification (τ = 20–40 s) due to very small diffusion distances of substrate to the TiO_2 surface in aerosol. The increase of the air RH from 4 to 37% (296 K) decreases the rate of adsorption but accelerates significantly the rate of photocatalytic oxidation. The complete air purification from organic compounds within 10 min is possible only with the photocatalytic oxidation because the adsorption alone does not remove methanol. The time needed for the air purification over the nanosized TiO_2 aerosol is directly determined by the rate of the aerosol generation which allows a further optimization of the TiO_2 aerosol air purification. The obtained results approve experimentally a suggestion that the photocatalytic oxidation over solid atmospheric aerosols actually takes part in the Earth atmosphere and serves as an important sink for airborne organics.

1. Introduction

Since the early works by Filimonov [1], McLintock et al. [2], Lyashenko and Gorokhovatsky [3] and N. Djeghri et al. [4], heterogeneous photocatalytic oxidation over oxides is considered as a powerful method of promoting the oxidative reactions in the gas phase. Environmental concerns of the last decades initiated the fruitful application of heterogeneous photocatalytic oxidation to purification of air. Numerous studies have demonstrated the ability of photocatalytic oxidation to provide mineralization of practically any organic compounds, i.e. their complete photocatalytic oxidation into stable inorganic products under certain exposure of the system with light [5]. The technology of photocatalytic oxidation over supported TiO_2-based photocatalysts located mainly in a fixed bed is now well developed and applied in a commercial scale for the purification of air from low concentrations of both organic and inorganic compounds [6–10].

The application of the fixed bed photocatalytic reactors for the air purification requires designing both the photocatalyst-support composites as well as the geometries of their irradiation with UV light to ensure good contact between the surface of the irradiated photocatalyst and the passing air stream. As to more active unsupported photocatalysts which are free from catalytically inactive supports, these are utilized mainly in reactors of two types. First, these are small-scale reactors which are used in research and operate usually at the low airflow rates that do not cause any sufficient mass transfer limitations for the unsupported photocatalysts. The second type of reactors are those with the fluidized bed of the photocatalyst that possesses a number of advantages over the fixed bed reactors. The advantages include

* Corresponding author. Tel.: +7 383 3269447; fax: +7 383 3331617.
E-mail address: voronts@catalysis.ru (A.V. Vorontsov).

0926-3373/$ – see front matter © 2009 Elsevier B.V. All rights reserved.
doi:10.1016/j.apcatb.2009.01.024

easy withdrawal and return of the photocatalyst for its regeneration as well as enhanced mass transfer. The fluidized bed gas phase reactors were employed for the photocatalytic oxidation of trichloroethylene [11–14], acetone [15], toluene [16], styrene [17], as well as removal of nitrogen oxides [18,9]. In such reactors, an enhancement of the photooxidation rate was observed in many cases experimentally that was explained by a decrease of effective irradiance as a consequence of the rotation of photocatalyst particles [15]. Common and well known disadvantages of the fluidized bed systems are the catalyst attrition and its carryover. The catalyst attrition makes an especially sufficient influence on photocatalytic reactions because of possibility of the light shading by the deposition of the attrition generated powders on the reactor windows or lamps used for illumination.

A particular type of the efficient and "global" fluidized bed photocatalytic reactors is known to be the Earth (and other planets) atmosphere where the photocatalyst can exist in the form of various aerosols [19–21]. However, the impact of the atmospheric heterogeneous photocatalytic reactions remains to be determined.

The possibility to provide photocatalytic oxidation at mild conditions of the environment as well as pronounced mass transfer parameters of fluidized bed or aerosol can be efficiently utilized for the emergency air purification from many airborne contaminants. Indeed, the fluidization of tiny photocatalyst particles under proper UV irradiation makes possible a quick decontamination of either indoor or outdoor air at the localized spots. In this work, we investigate the possibilities for the quick air purification from vapors of acetone and simulant chemical agent dimethyl methylphosphonate (DMMP) with the help of an aerosolized TiO_2 powder affected by UV irradiation.

The adsorption of both compounds on the photocatalyst surface is evidently the first stage which precedes their photocatalytic oxidation. Note, however, that in contrast to acetone, DMMP is known to be able of the irreversible reactive adsorption over anatase TiO_2 [22–24]. The reactive adsorption over TiO_2 was observed also for some other compounds like diisopropyl fluorophosphonate [25], 2-chloroethyl ethylsulfide [26], etc. The ability of such irreversible adsorption over TiO_2 can accelerate sufficiently the process of the emergency air purification.

Investigation of toxic effects of nanoparticles is currently a subject of intensive research. It has been recently found that inhalation of an aerosol of nanosized TiO_2 particles can cause inflammatory response in mice lungs [27]. Therefore, TiO_2 aerosol should be used with caution for air purification in the presence of living things. This method can be, however, indispensable for very quick alleviation of lethal or severe exposures to toxic compounds since the inflammatory aftermath of a TiO_2 aerosol is much better than heavy or lethal health effects of the toxic compounds.

We applied fluidization of the UV irradiated anatase TiO_2 powder in a closed chamber to attain quick air purification. In contrast to traditional fluidized bed experiments with photocatalyst granules of sizes above tens of micrometers, the characteristic size of TiO_2 particles in our study was below 2 μm. Such small particles behave like aerosols. Since the concentration of such particles in the generated dusty cloud was large enough, the characteristic distance that substrate molecules travel before they collide with a TiO_2 particle is small. This diminishes the external diffusion time very much and accelerates largely the substrate adsorption. Also, the very small sizes of the TiO_2 particles makes the time of their precipitation long enough to allow the deep photocatalytic oxidation over aerosolized TiO_2 particles. The present study expands and details our preliminary experiments on TiO_2 aerosol [28] and provides careful discussion of the results.

2. Experimental

2.1. Materials

The photocatalyst powder applied for the reactions was TiO_2 Hombikat UV 100 (anatase 100%) with specific surface area approximately 320 m^2/g and the primary particles size 5 nm [15]. Before generating the aerosol, the TiO_2 powder was dried overnight at 120 °C; this procedure was found to be important for the efficient aerosol formation. Acetone (Reachim) and dimethyl methylphosphonate (98% Sigma–Aldrich) were used as received.

2.2. Reaction setup and methodology

The experimental setup is schematically shown in Fig. 1. The core of the setup is a 100 l cubic Plexiglas chamber. An aerosol generator is placed in the middle of the chamber floor, while a 22 W annular UV fluorescent mercury lamp TL-E/10 (Philips) is located at the center of the chamber. According to the manufacturer specifications, the radiant power emitted by this lamp in the UV region is $P = 3.9$ W. The lamp emission spectrum has an intensive maximum at wavelength 365 nm, the half-height width of the spectral line is 20 nm. This band completely falls into the TiO_2 band gap absorption region ($\lambda < 400$ nm). The photon flux of this band is $\Phi = 1.2 \times 10^{-5}$ Einstein s^{-1} as calculated with the expression

$$\Phi = P\frac{\lambda \times 10^{-9}}{N_A hc}$$

where λ is average wavelength of irradiation (nm), N_A is the Avogadro number (mol^{-1}), h is the Planck constant (J s), and c is the speed of light in vacuum (m s^{-1}).

UV irradiance ($\lambda < 400$ nm) was also determined experimentally using a radiometer and an UV cut-off filter at the center of a wall as 1.6 W/m^2 and at the center of the ceiling of the chamber as 3.4 W/m^2. Integration over the chamber surface gives an estimate of the total UV radiant power of 2.7 W that reasonably agrees with the manufacturer's specification.

Primary quantum efficiency of substrate consumption steps of photocatalytic processes was estimated using the standard formula [29]

$$\varphi = \frac{W_N}{\Phi} \quad (1)$$

where W_N is the rate of the substrate consumption on amount basis (mol s^{-1}) calculated from a concentration–time plot, Φ is the

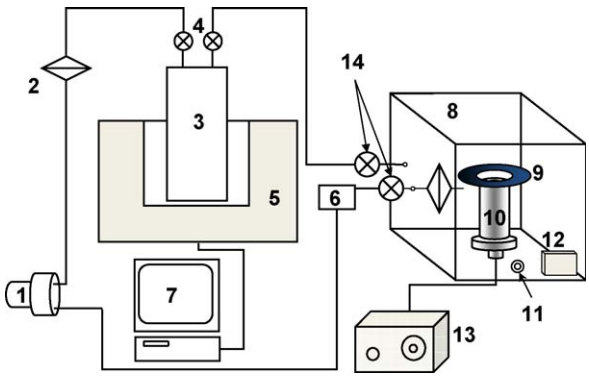

Fig. 1. Scheme of the experimental setup. (1) Membrane circulation pump, (2) 0.2 μm membrane filter, (3) long-path IR gas cell, (4) valves, (5) FT-IR spectrophotometer Vector 22 (Bruker), (6) humidity meter, (7) computer connected to FT-IR, (8) chamber, (9) UV lamp, (10) aerosol generator, (11) sampling & injection port, (12) digital thermometer, (13) signal generator, (14) spherical stopcocks.

incident photon flux (E s^{-1}) according to the lamp manufacturer's specification. Overall quantum efficiency of photocatalytic oxidation into inorganic products was calculated with the next equation:

$$\varphi = m\frac{W_N}{\Phi} \quad (2)$$

where W_N is the rate of reaction of deep oxidation into inorganic products, Φ is the incident photon flux, m is the assumed number of photons needed for the deep oxidation, m = 16 for the acetone and 20 for the DMMP oxidation.

The design of the aerosol generator is analogous to that of the vibrofluidized bed reactor described in detail in [15]. The TiO_2 powder is fluidized inside a plastic cylinder with 15 cm length and 7 cm diameter with a speaker. The TiO_2 aerosol is emitted into the chamber space from a small orifice (Ø 5 mm) in the plastic cylinder. The speaker membrane operated at a 5 W power with a frequency of 200 Hz.

5 g of TiO_2 powder was placed over the speaker membrane in the aerosol generator before each experiment. The chamber was then sealed and purged with air of the required relative humidity through the inlet and outlet ports. The aerosol generator internal air was isolated from the chamber space with an aluminum foil to prevent the substrate adsorption and reactions over TiO_2 inside the generator before it sprays the photocatalyst into the chamber air. After the required relative humidity of the chamber air is stabilized, the liquid substrate is injected into the chamber injection & sampling port with a Hamilton syringe. The volume of the injected acetone and DMMP was 91 and 45 μl, respectively. These amounts of acetone and DMMP correspond to the gas phase concentration of 304 and 102 ppm, respectively. The port is equipped with an electric heater to provide quick evaporation of DMMP. Unless otherwise stated, the release of the TiO_2 aerosol was started after the substrate vapor concentration reaches a steady value. The TiO_2 powder was aerosolized by 96% during 10 min. Thereafter electrical power of the aerosol generator was turned off and the experiment continued with both aerosolized and precipitated TiO_2. In the photocatalytic experiments, the UV lamp was switched on before the start of the aerosol generation. In the adsorption experiments, the UV lamp was not energized.

2.3. Analysis

The concentration of gaseous organic compounds and CO_2 in the chamber air was measured by means of an FT-IR spectrometer Vector-22 (Bruker) equipped with a long path gas cell G-3-8-H (Infrared Analysis Inc.). Air from the chamber circulated continuously through the infrared cell with the use of a 5 dm^3/min membrane pump. The response time of the chemical analysis system which monitored the changes in the chamber's gas phase composition was proved to be ca. 15 s. The water vapor content in the chamber air was adjusted to low values by passing the air through silica gel. The relative humidity of air was determined by a humidity meter that was included into the sampling circle. The concentration calibrations for the compounds to be analyzed were done by passing a flow of air with the known concentration of these compounds through the IR cell. Since DMMP is capable of adsorption onto the Plexiglas chamber walls, the exact calibration required the continuous flow of air with injecting DMMP using a Cole Parmer syringe pump. The concentrations were confirmed by GC measurements using a LHM-8 M instrument (Russia) equipped with an FID and methanator. The following bands were used for the concentration measurements with IR spectroscopy: 1150–1275 cm^{-1} for acetone; 950–1150 cm^{-1} for DMMP and methanol; 2200–2450 cm^{-1} for CO_2. The spectra were measured from 450 to 4000 cm^{-1} at resolution 4 cm^{-1}. Each spectrum represents an average of 5 scans.

The measurements of the TiO_2 particle size distribution and overall concentration inside the experimental chamber were performed with a Handheld 2016 instrument (Lighthouse Worldwide Solutions). The instrument measures particles concentration in the ranges of sizes 0.2–0.3, 0.3–0.5, 0.5–0.7, 0.7–1, 1–2 and >2 μm. Air from the chamber was supplied to the instrument with dilution by pure air of about 1000^x to insure the validity of the measurements in the working range of the particles counter.

3. Results and discussion

3.1. Aerosol characteristics

The sonic generator of the TiO_2 aerosol has not been studied in detail before. Therefore it is important to check the major characteristics of the experimental system shown in Fig. 1. After turning on the electrical feed to the aerosol generator, it starts emitting the TiO_2 aerosol through the orifice in its top. In 10 min, 95–98% of TiO_2 loaded in the generator is sprayed. Thereafter the generation of the aerosol proceeds at a very low speed. The aerosol generator was turned off after 10 min of the operation. Experimentally determined mass of the sprayed TiO_2 as a function of time fits well to the equation:

$$m(t) = -0.0298t^2 + 0.7728t, \quad (3)$$

where t is time (min), $m(t)$ is the mass of the sprayed TiO_2 (g). The mass of the sprayed TiO_2 was measured by weighing the aerosol generator loaded initially with the same mass of TiO_2 after different periods of aerosol generation.

The typical mass of TiO_2 sprayed during 10 min operation is 4.8 g. The visual observation of air inside the chamber (Fig. 1) shows that the TiO_2 aerosol is opaque after 5 min of the aerosol release. At the moment of the aerosol maximum concentration it is not possible to observe the opposite wall of the chamber. Light scattering by the aerosol particles is observable even in 60 min after turning off the aerosol generator.

Absorption of light of the UV lamp by the aerosol particles was estimated by measuring UV irradiance ($\lambda < 400$ nm) at the chamber ceiling. It turned out that the UV irradiance decreased during the aerosol spraying. The highest fraction of UV light absorbed corresponded to 40% at t = 10 min. Thereafter, UV light absorption gradually decreased to about 20% and did not changed then. This absorption is caused by the TiO_2 powder deposited over the UV lamp.

Quantitative characteristics of the aerosol produced were obtained with the aerosol particles counter. The maximum concentration of the aerosol was reached after 10 min of the aerosol generator operation. The aerosol particles concentration decreased twice approximately in 40 min after the initiation of the TiO_2 aerosol production. This time is long enough to allow carrying out the adsorption and photocatalytic experiments over the particles mainly in the aerosol state.

Fig. 2a demonstrates the aerosol particles size distribution at the moment of the maximum aerosol concentration. One can see in Fig. 2a that the majority of aerosol particles have diameter about 0.2–0.3 μm. The overall concentration of TiO_2 particles was as high as 1.5×10^6 cm^{-3}. For adsorption and catalytic processes, the most important characteristic of the aerosol particle is not its diameter but the surface area of the TiO_2 material inside it that is available for adsorption and catalysis. Fig. 2b shows the distribution of the surface area of TiO_2 material inside aerosol particles per unit of air volume over different aerosol particle sizes. One can obtain the overall surface area of aerosol particles with different diameter,

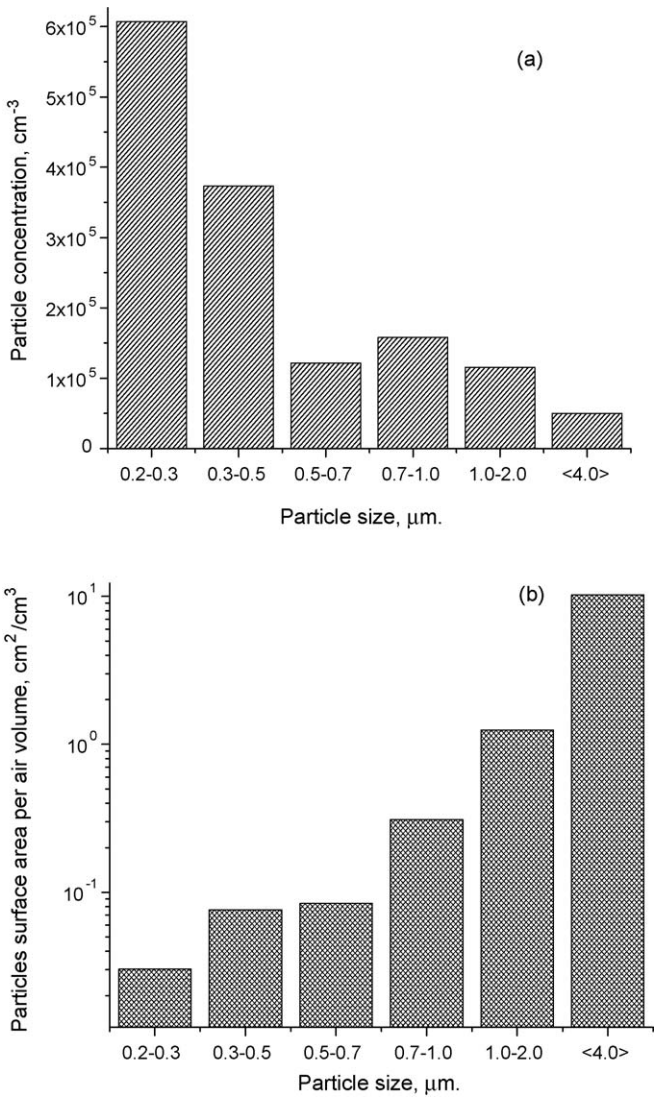

Fig. 2. Distribution of TiO_2 aerosol particles concentration (a) and TiO_2 material surface area per air volume (b) over particles sizes.

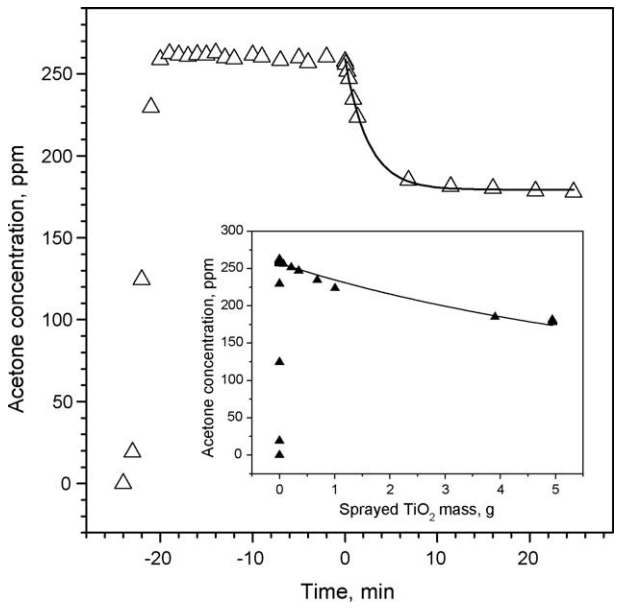

Fig. 3. Dynamics of the acetone concentration change during the dark adsorption experiment at air humidity 37 ± 3%. The injection of acetone was done at $t = -24$ min, the aerosol generation started at $t = 0$ min. The inset shows the effect of the sprayed TiO_2 mass on the acetone concentration and its approximation by Eq. (6).

which is available for adsorption, by multiplying data in Fig. 2b by the experimental chamber volume (10^5 cm^3). The surface area of TiO_2 material inside particles is proportional to the TiO_2 mass, which in turn is proportional to the third power of their diameter. Thus, the majority of the aerosol surface area resides in the largest aerosol particles. It is the particles with size above 2 μm that have the highest influence on adsorption and catalytic processes provided there is no strong internal diffusion limitation inside the particles.

3.2. Adsorption of acetone

Air humidity can influence significantly the adsorption and photocatalytic oxidation of organic vapors. In the present study, two levels of the air humidity were employed for the experimentation—37 and 4%. At the temperature of the experimental chamber 296 K these humidity levels correspond to the water vapor concentration about 10,300 and 1000 ppm, respectively. Since water molecules compete for the adsorption sites with organic molecules, one can expect a significant effect of humidity on both the adsorption and photocatalytic oxidation over TiO_2 aerosol.

Fig. 3 shows the changes of the acetone concentration in an adsorption experiment at RH 37%. After the injection of liquid acetone and its evaporation, the acetone concentration stabilizes inside the chamber at about 260 ppm. At the moment $t = 0$ min, the aerosol generator was switched on and the aerosol concentration started to increase. As a result of adsorption over TiO_2 aerosol particles, the acetone concentration fell to 180 ppm at the moment $t = 10$ min. Since the aerosol release finished at $t = 10$ min, the acetone concentration keeps steady at this level thereafter. In total, about one third of the acetone was removed from the gas phase owing to the adsorption.

The acetone concentration decay in Fig. 3 is well fitted by the following single exponential decay

$$C = 180 + 80\,e^{-t/2.5}$$

where C is acetone concentration (ppm), t is the experiment time (min). The solid line of the concentration decay in Fig. 3 was plotted according to this function. Table 1 lists characteristic time of the acetone concentration decay during the adsorption experiments. Thus, the acetone concentration decrease as a result of its adsorption over TiO_2 aerosol is well described by a single exponential decay with characteristic time $\tau = 2.5$ min.

The adsorption experiment like that in Fig. 3 represents an alternative approach to measuring the adsorption isotherms. The traditional approach consists in placing a fixed amount of adsorbent and changing the concentration of a substance to be adsorbed. With continuous spraying of TiO_2 into the experimental volume, we actually kept constant the total amount of the substance to be adsorbed while increasing the amount of adsorbent. Since the dependence of the sprayed TiO_2 mass on the experiment time is known and given by Eq. (3), one can obtain the plot of the gas phase adsorbate concentration vs. the amount of the adsorbent added. The inset in Fig. 3 shows the acetone concentration as a function of the sprayed TiO_2 mass. Zero TiO_2 mass corresponds to the injected acetone evaporation and stabilization of its concentration. The decrease of the acetone concentration with the increase of sprayed TiO_2 mass corresponds to acetone adsorption over the TiO_2 aerosol particles.

Table 1
Characteristic time and consumption of acetone at the purification of air from acetone vapors in the dark.

Figure number	Relative humidity (%)	Characteristic time of adsorption τ_1 (min)	Consumption of acetone by the adsorption at $5\tau_1$ (%)
Fig. 3	37 ± 3	2.5 ± 0.1	31
Fig. 4	4 ± 1	2.5 ± 0.1	82

For the quantitative description of this dependence, one can use an assumption that the adsorption of acetone is at equilibrium at every moment of an experiment. Then we can use the traditional Langmuir adsorption isotherm:

$$a = a_m \frac{KC}{1 + KC} \tag{4}$$

where a is the amount of adsorbate (mol), a_m is the monolayer adsorption (mol), K is the adsorption equilibrium constant (ppm^{-1}) and C is the concentration of the substance in the gas phase (ppm). By expressing the amount of the adsorbate through the initial, C_0 and current, C, gas phase concentration and performing the required dimensions transformations we get the equation:

$$\alpha(C_0 - C) = Nm(t) \frac{KC}{1 + KC} \tag{5}$$

where N is the adsorption site mass density (mol sites g^{-1}), $m(t)$ is the mass of adsorbent as a function of experiment time (g), α is the dimension transformation coefficient (mol ppm^{-1}), $\alpha = 10^{-6}(PV/RT) = 4.09 \times 10^{-6}$, P is the pressure (Pa), V is the reaction system volume (m^3), R is the universal gas constant (J K^{-1} mol^{-1}), T is the absolute temperature (K). The solution of quadratic Eq. (3) with respect to C gives expression

$$C = 0.5[C_0 - \beta m - \kappa + \sqrt{(\kappa - C_0 + \beta m)^2 + 4\kappa C_0}], \tag{6}$$

where $\beta = N/\alpha$ (ppm g^{-1}), $\kappa = 1/K$ (ppm).

Eq. (6) was fitted to the experimental points in the inset in Fig. 3 and the curve was plotted according to the fit results. The curve satisfactorily describes the experimental data. The obtained parameters are $\beta = 280 \pm 20$ ppm g^{-1} and $\kappa = 2830 \pm 207$ ppm. They correspond to the adsorption site density $N = 0.011$ mol g^{-1} and adsorption constant $K = 0.00037$ ppm^{-1}. The calculated adsorption site area for the acetone molecule 0.46 nm^2 is reasonable and agrees with the previously reported values of 0.6 [30] and 0.4 nm^2 [31]. The saturation acetone monolayer density for dehydrated TiO_2 was reported to be 10 nm^{-2} [32], whereas the Ti^{4+} cations surface density for the (1 1 0) face of TiO_2 was reported to be 5.2 nm^{-2} [33].

Decreasing the air RH to 4% results in marked changes of the acetone adsorption over TiO_2 aerosol. Fig. 4 shows that the initial acetone concentration 260 ppm fell down to 45 ppm after 10 min of the TiO_2 spraying. The decrease of the DMMP concentration is described well by the following single exponential decay kinetics

$$C = 45 + 211\, e^{-t/2.5}$$

The decay line in Fig. 4 is plotted according to this kinetics. Table 1 shows that the acetone removal characteristic time is the same for RH 37 and 4%. However, adsorption at RH 4% results in removal of ca. 80% of the initial gas phase acetone by the TiO_2 aerosol surface.

After the TiO_2 spraying had been stopped at $t = 10$ min, the acetone concentration decrease stopped too. This shows that the time for the equilibration of the acetone adsorption is much lower than 0.5 min. Thus, the derived model that results in Eq. (6) is sound. The inset in Fig. 4 demonstrates the dependence of the acetone concentration on the sprayed TiO_2 mass. Experimental

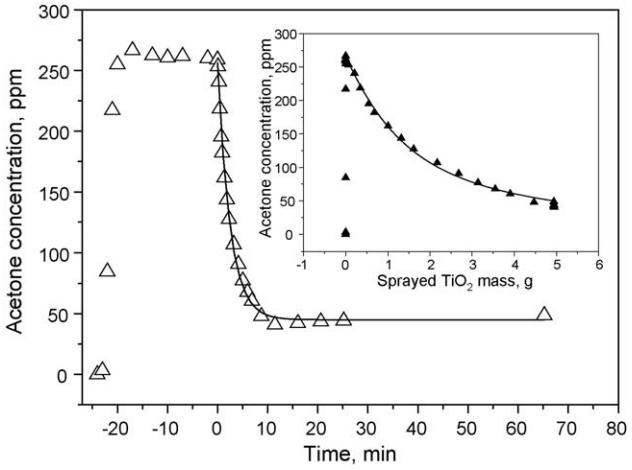

Fig. 4. Dynamics of the acetone concentration during the dark adsorption experiment at air humidity 4 ± 1%. The injection of acetone was done at $t = -24$ min, the aerosol generation started at $t = 0$ min. The inset shows the effect of the sprayed TiO_2 mass on the acetone concentration and its approximation by Eq. (6).

points were fitted to Eq. (6) and the curve demonstrates the result. One can see that Eq. (6) describes the experimental points very well. The adsorption parameters magnitudes determined from the fit are $\beta = 280 \pm 50$ ppm g^{-1} and $\kappa = 271 \pm 68$ ppm. The adsorption isotherm parameters calculated from them are the adsorption sites density 2.14 nm^{-2} and the adsorption constant $K = 0.0037$ ppm^{-1}. Note that, as expected, the adsorption site density was unchanged but the adsorption constant increased significantly upon the decrease of water vapor concentration. The obtained values $K = 0.00037$ ppm^{-1} at RH 37% and $K = 0.0037$ ppm^{-1} at RH 4% agree satisfactorily with the previously reported $K = 0.0026$ ppm^{-1} at RH 15% [30].

Previously it was shown [34] that the competitive adsorption of acetone in the presence of water can be described within the Langmuir model by substitution of the adsorption constant by the following function:

$$K = \frac{K_a}{1 + K_{H_2O} C_{H_2O}} \tag{7}$$

where K_a is the substrate adsorption constant (ppm^{-1}), K_{H_2O} is the water adsorption constant (ppm^{-1}) and C_{H_2O} is the water vapor concentration (ppm). By solving the system of Eq. (7) for the two investigated humidity levels we obtain the intrinsic acetone adsorption constant $K_a = 0.11$ ppm^{-1} and the water adsorption constant $K_{H_2O} = 0.03$ ppm^{-1}. Sauer and Ollis previously reported acetone and water adsorption constants for a TiO_2-monolith system equal to 0.5 and 0.0075 ppm^{-1}, respectively [35]. These values are of the same order of magnitude as those in the present study.

3.3. Photocatalytic oxidation of acetone

The adsorption over TiO_2 aerosol results in only incomplete purification of air from the acetone vapor due to low values of the adsorption constant. However, the adsorption equilibrium can be sufficiently shifted by the removal of the adsorbate from the gas phase in a mild oxidation process such as the photocatalytic oxidation.

Fig. 5 shows the kinetics of the acetone and CO_2 concentration changes at the photocatalytic oxidation of acetone over sprayed TiO_2 at RH 37%. Analogously to experiments in Section 3.2, acetone concentration increases and stabilizes after the liquid acetone

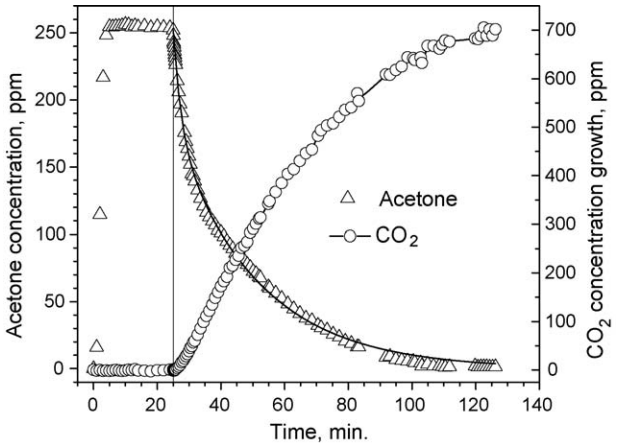

Fig. 5. Photocatalytic oxidation of the acetone vapor at relative humidity 37 ± 3%. Acetone was injected at t = 0 min, the aerosol generation start at t = 25 min is marked with a vertical line. The acetone concentration decrease is approximated with a double-exponential decay.

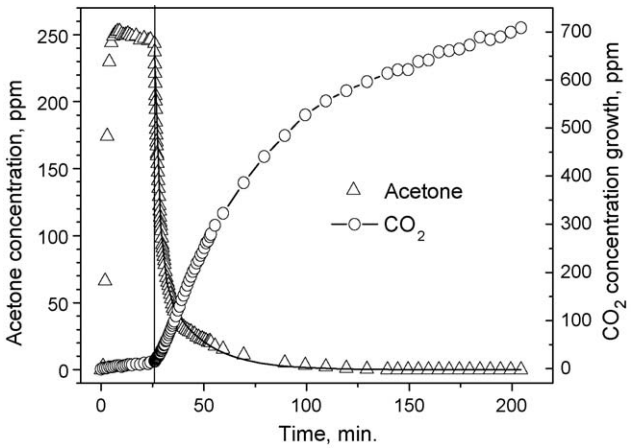

Fig. 6. Photocatalytic oxidation of the acetone vapor at relative humidity 4 ± 1%. Acetone was injected at t = 0 min, aerosol generation started at t = 26 min (vertical line). The acetone concentration decrease is approximated with a double-exponential decay.

injection. The decrease of the acetone concentration after the aerosol production start is well described by the following double-exponential decay function plotted in Fig. 5:

$$C = 73\,e^{-t/2.5} + 179\,e^{-t/26.2}$$

Table 2 summarizes the characteristic times, CO_2 formation rate and extent of the air purification by the acetone photocatalytic oxidation. The rate of CO_2 formation was calculated from the initial linear part of the CO_2 concentration growth. The acetone adsorption proceeds with the same characteristic time τ_1 = 2.5 min as in the case of the dark adsorption. The characteristic time of photocatalytic oxidation τ_2 is one order of magnitude longer. Since the aerosol lifetime is about 40 min counting from the start of the aerosol generation, the major changes of the concentrations corresponding to photocatalytic oxidation take place with the participation of the aerosolized TiO_2 particles. The decrease of the acetone concentration after 10 min of the UV illumination was about 55% of its starting value 260 ppm. This is about twice larger than at the air purification with the help of the "pure" adsorption. About 14% of the stoichiometric amount of CO_2 was formed during this time interval. Thus, only one half of the acetone removal acceleration is caused by deep photocatalytic oxidation. The rest of the acetone removal rate seems to be due to other photocatalytic processes such as acetone photoadsorption and incomplete oxidation of acetone molecules with the formation of compounds with the larger adsorption constant. The primary quantum efficiency of the acetone consumption during the first 10 min is estimated with Eq. (1) as 3.4%. The air purification from acetone was finished by 99% in 80 min from the start of the aerosol release. Mineralization of the initially injected acetone into CO_2 was completed by 80% after 100 min of irradiation. There is little doubt that the mineralization would be completed if the irradiation were continued.

The photocatalytic oxidation of the acetone vapor at RH 4% results in the kinetic curves shown in Fig. 6. The acetone concentration decrease due to adsorption and photocatalytic oxidation is well fitted by the following function plotted in Fig. 6:

$$C = 164\,e^{-t/2.3} + 73\,e^{-t/19}$$

The characteristic time of the acetone removal by adsorption τ_1 = 2.3 min was the same as in the corresponding dark process and the characteristic time of the acetone removal by photocatalytic oxidation τ_2 was close to that at RH 37% (Fig. 5). It is interesting that the removal of the acetone vapor at the first 10 min of the reaction under UV irradiation proceeded by the same degree as in the adsorption experiment. Obviously at RH 4%, the adsorption dominates over the oxidation during this period. In contrast to our previous results [15], the decrease of the water vapor concentration led to a decrease of the deep oxidation rate measured directly by the rate of the CO_2 formation (see Table 2). Two opposite tendencies – the decrease of the rate of the deep photocatalytic oxidation and the increase of the adsorption rate – summed up in the same time of the air purification from acetone vapor by 90% equal to 80 min counted from the start of aerosol release. However, mineralization of the initially injected acetone into the gas phase CO_2 went slower compared to the case of the higher RH and reached 80% only after 180 min of irradiation.

3.4. Adsorption of DMMP

The DMMP structure and physical properties resemble those of chemical agents but DMMP has only very low toxicity. For this reason, the dimethyl methylphosphonate adsorption and photocatalytic oxidation over TiO_2 have been studied relatively well. DMMP molecules adsorbed over the anatase surface undergo reaction with surface that leads to hydrolysis of a single methoxy

Table 2
Parameters of the air purification from acetone under UV radiation.

Figure number	Relative humidity (%)	Characteristic time of adsorption and photocatalysis (min)		Consumption by the adsorption and photocatalysis (%)		Initial rate of CO_2 formation (ppm/min)
		τ_1	τ_2	$2\tau_1$	$5\tau_2$	
Fig. 5	37 ± 3	2.5 ± 0.2	26.2 ± 0.5	53	100	12.9
Fig. 6	4 ± 1	2.3 ± 0.1	19 ± 1	70	100	9.8

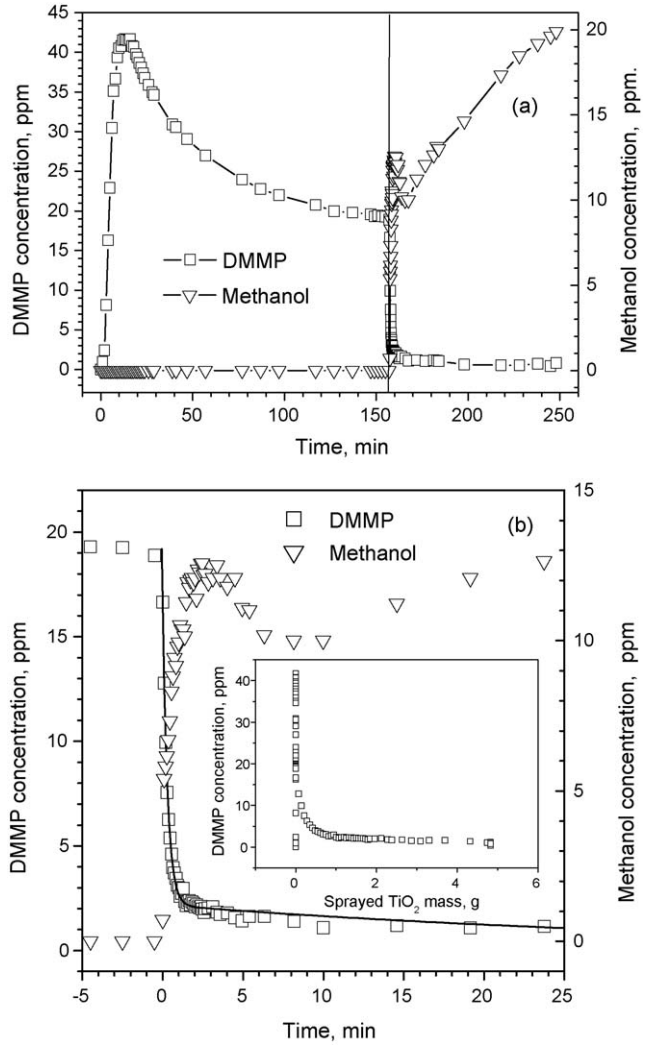

Fig. 7. (a) Dynamics of the DMMP and methanol concentration during dark DMMP adsorption experiment at air humidity 37 ± 3%. DMMP was injected at $t = 0$, the aerosol release start at $t = 157$ min is marked with a vertical line. (b) Magnified part of the plot corresponding to the fast adsorption and hydrolysis period. DMMP concentration decrease is approximated with a double-exponential decay. The start of the aerosol production is at $t = 0$ min. The inset shows the effect of the sprayed TiO_2 mass on the DMMP concentration.

group into methanol and methyl methylphosphonic acid. This transformation makes the DMMP adsorption irreversible.

In the present study, interaction of the DMMP vapor with TiO_2 aerosol was studied at two air relative humidity levels—37 and 4% (296 K). High boiling point and polarity of DMMP on one hand makes this object very easy to remove from gas phase but on another hand creates significant complications of kinetic studies of its transformation due to the DMMP interaction with some equipment components.

Fig. 7a shows the kinetics of the concentration changes of gas phase DMMP and methanol in the adsorption experiment at RH 37%. After the injection of liquid DMMP, it evaporates and the DMMP concentration in gas phase increases. Then the DMMP concentration reaches a peak and decreases gradually due to the adsorption and/or absorption on some units of the experimental chamber. In 2–3 h after the injection, the DMMP concentration stabilized and the TiO_2 aerosol generation could be started. It was important to wait till the DMMP concentration reaches a steady value because the interaction with equipment would obscure the adsorption over TiO_2 aerosol.

After starting the TiO_2 spraying, decline of the DMMP concentration was so fast that it is necessary to plot it in a separate figure to make clearly visible. Fig. 7b shows that simultaneously to the DMMP adsorption, gas phase methanol appeared in the chamber's air. The DMMP concentration dynamics is well described by a double exponential decay that was plotted in Fig. 7b. The characteristic times of DMMP and methanol removal, consumption of DMMP and rates of methanol formation during the DMMP adsorption are listed in Table 3. The first exponent with the characteristic time $\tau_1 = 0.7$ min describes the decay of DMMP concentration from the starting value to ~1 ppm. This decay is due to the very fast adsorption. The second exponent describes the further slower decay of the DMMP concentration. Since error in DMMP concentration determination is comparable to 1 ppm, τ_2 has a large error too. We believe that the characteristic time τ_1 corresponds to the "pure" DMMP adsorption over TiO_2 aerosol particles whereas the much longer time τ_2 corresponds to the processes of the DMMP desorption from the chamber's walls and its adsorption over TiO_2. If there were no such desorptive interference, the DMMP concentration would decrease by 99% in as short time as 3.2 min.

The inset in Fig. 7b represents the DMMP concentration as a function of the sprayed TiO_2 mass. Since the adsorption of DMMP is irreversible, this dependence cannot be described by Eq. (6). Under assumption of irreversible DMMP adsorption $KC \gg 1$, the Langmuirian model (5) transforms in this case into the next equation

$$\alpha(C_0 - C) = Nm(t)$$

The fit to the experimental points was done with the linear equation

$$C = C_0 - \beta m(t) \quad (8)$$

However, the significant curvature of the dependence in the inset in Fig. 7b evidences that Eq. (8) is not suitable for description of the DMMP adsorption over the TiO_2 aerosol. One of the possible reasons for this lies in a slow desorption from the chamber walls. However, the further consideration shows that there may be other reasons.

Fig. 7b shows that gaseous methanol forms immediately after the start of the TiO_2 aerosol release. The characteristic time of the methanol release is about 0.6 min which matches perfectly the characteristic time of the DMMP removal by adsorption. Thus, the inherent hydrolysis characteristic time is much shorter than 0.6 min. The DMMP hydrolysis seems to take place immediately after adsorption of DMMP on TiO_2 particles. This differs drastically with the previous results of the DMMP adsorption and hydrolysis

Table 3
Parameters of the air purification from the DMMP vapors in the dark.

Figure number	Relative humidity (%)	Characteristic time of DMMP removal (min)		Consumption of DMMP (%)		Initial rate of methanol formation (ppm/min)	Characteristic time of methanol consumption (min)	Long time rate of methanol generation (ppm/min)
		τ_1	τ_2	$2\tau_1$	$2\tau_2$			
Fig. 7	37 ± 3	0.7 ± 0.1	91 ± 84	83	94	4.9	7.8 ± 0.4	0.12
Fig. 8	4 ± 1	0.3 ± 0.1	15 ± 10	79	~100	8.7	1.7 ± 0.2	0.025

over the film of the same TiO_2: the time of hydrolysis (~250 min) was one order of magnitude longer than the adsorption time (20 min) [24]. Methanol concentration reaches a maximum value of ~13 ppm in ~3 min after the start of aerosol generation. Then it decreases by ~3 ppm, reaches a minimum at $t \sim 10$ min and increases slowly again. The decrease is associated with adsorption of methanol on fresh portions of generated aerosol. The slow increase of the methanol concentration (Fig. 7a) shows that a part of DMMP undergoes quick hydrolysis but another part hydrolyzes very slowly: methanol formation does not stop even in 100 min. The average rate of the methanol generation is given in Table 3. Thus, it is possible that the previously reported characteristic time of DMMP hydrolysis corresponds to the slow hydrolysis of the present study.

Fig. 8a shows the DMMP and methanol concentration curves during the DMMP adsorption over the TiO_2 aerosol at RH 4%. In this case, the adsorption over the internal surfaces of the experimental equipment proceeded to an even higher extent. This can be explained by the decrease of the water competition for the adsorption sites. In ca. three hours, the DMMP concentration stabilized and the generation of the TiO_2 aerosol was started. The concentration of the DMMP vapor underwent a drastic decrease accompanied by a quick increase of the gas phase methanol concentration that is clearly seen in Fig. 8b. In 0.6 min after starting the TiO_2 aerosol generation, the concentration of methanol reaches a maximum and then decreases exponentially with characteristic time 1.7 min (Table 3). This decrease is several times faster than at RH 37% due to the faster removal of gas phase DMMP because of decrease of the adsorption competition with water vapor. The first characteristic time τ_1 of the DMMP concentration exponential decay was as low as 0.3 min. This time is very close to the characteristic time of measuring the concentration changes in the chamber. Thus, the adsorption was so fast that the first few points of the concentration decay even fell out of the decay curve.

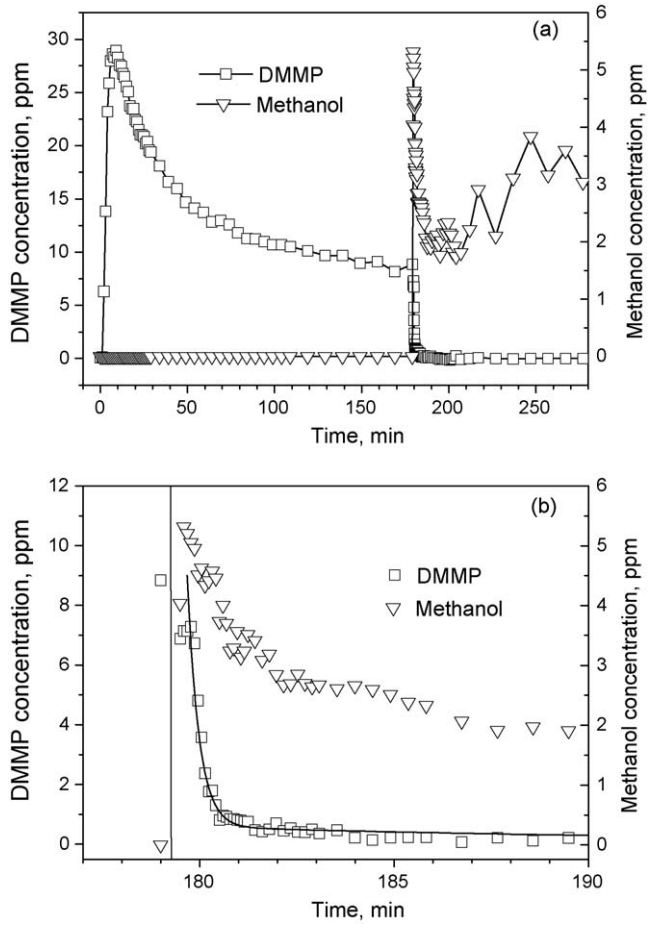

Fig. 8. (a) Dynamics of the DMMP and methanol concentration during dark DMMP adsorption on particles of titanium dioxide aerosol at air humidity 4 ± 1%. DMMP was injected at $t = 0$ min, the aerosol release was started at $t = 179$ min. (b) Magnified part of the plot corresponding to the fast adsorption and hydrolysis period. The vertical line marks the start of the aerosol release. The DMMP concentration decrease is approximated with a double-exponential decay.

The high initial rate of the air purification confirms the expectations that small distance between particles in TiO_2 aerosol would enable very quick diffusion transport of the substrate gas phase molecules to the adsorption sites. The rate of the gas phase compounds removal is actually limited by the rate of the TiO_2 aerosol generation. In our case the latter was a relatively slow process. However, in case if an explosive generation of the TiO_2 aerosol would be applied, the characteristic time of the air purification could reach sub-second ranges.

3.5. Photocatalytic oxidation of DMMP

It is demonstrated in the previous section that adsorption appears to be a fast method of air purification from the chemical warfare agent simulants. However, there are several problems with this method. First, it does not provide an irreversible destruction of organic substrates. The second issue is that toxic gaseous by-products can be generated continuously over long time after the adsorbent application. Figs. 7b and 8b show that a toxic compound like methanol is released from the adsorbent even hours after starting the TiO_2 aerosol spraying.

The photocatalytic oxidation is expected to decompose any organic compounds into inorganic ones. Fig. 9a shows results of air purification by the TiO_2 aerosol under irradiation with the 22 W toroidal UVA lamp at RH 37%. The behavior of the DMMP concentration before the start of TiO_2 spraying was obviously the same as in the "pure" adsorption experiments. DMMP did not undergo photolysis in the absence of TiO_2. Table 4 in comparison with Table 3 demonstrates that the characteristic time τ_1 of the double exponential decay of DMMP concentration changed insignificantly in transition from pure adsorptive to adsorptive-photocatalytic purification. Adsorption clearly provides the major part of the DMMP removal from the gas phase.

The kinetic curves of the harmful byproduct, methanol, demonstrate a drastic difference between the adsorption and adsorption-photocatalytic experiments. In the pure adsorptive process, the methanol concentration quickly reaches a maximum, then decreases by few ppm, and then steadily increases over a long time. Fig. 9b shows that in the photocatalytic oxidation, the methanol concentration reaches a maximum in 1 min after the start of the TiO_2 aerosol generation and then in 10 min decreases to the value below the detection threshold (0.5 ppm). Thus, in contrast to adsorption, photocatalytic oxidation results in the complete air purification in about 10 min. Simultaneously, CO_2 is produced in the gas phase and the conversion into CO_2 of the initially injected DMMP attains 85% at 400 min after starting the TiO_2 release. 100% mineralization of the injected DMMP corresponds to CO_2 concentration 300 ppm.

Fig. 10a depicts the adsorption-photocatalytic air cleaning at air RH 4%. Again, the DMMP concentration evolution in time is very similar to that in the pure adsorption experiment. The decrease of RH results in the nearly double decrease of the characteristic DMMP removal time τ_1 (Table 4). The methanol concentration reaches a maximum in 1 min after

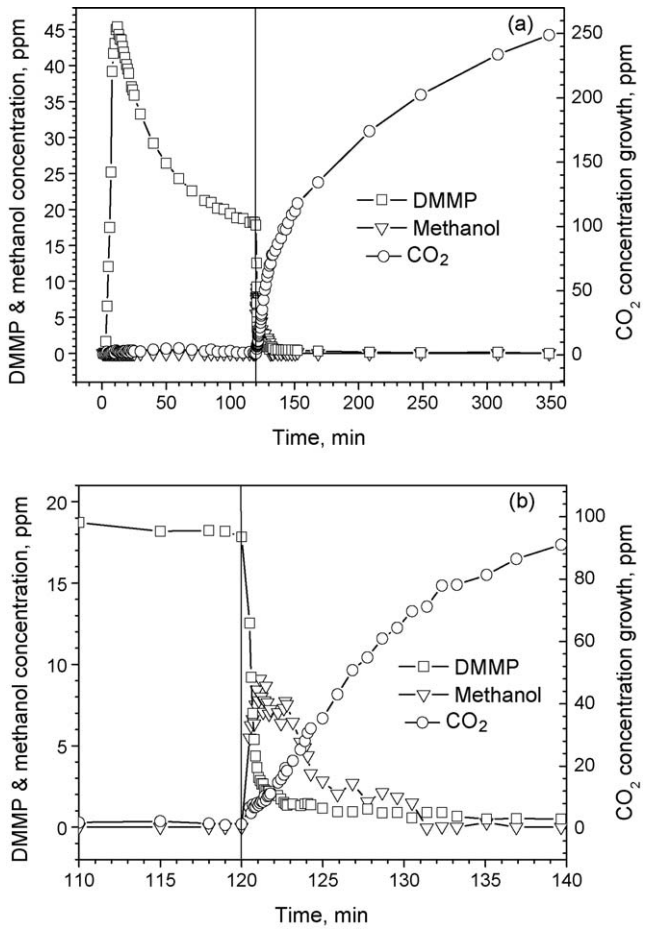

Fig. 9. (a) Temporal concentration profiles at the simultaneous adsorption and photocatalytic oxidation of DMMP under air humidity 37 ± 3%. The injection of liquid DMMP was done at t = 0 min, the TiO_2 aerosol generation started at t = 120 min (vertical line). (b) Magnified part of the plot corresponding to the fast adsorption and hydrolysis period.

the start of the TiO_2 aerosolization and decreases to below 0.5 ppm by 6 min. The faster rate of the methanol removal from the chamber's air should be attributed to its stronger adsorption over new portions of sprayed TiO_2 at lower RH. The profile of the CO_2 concentration and data in Table 4 testify that the deep photocatalytic oxidation actually proceeds at the about twice lower rate at RH 4%. The initial rate of the CO_2 generation is lower by a factor of 2 and mineralization of the initially injected DMMP into CO_2 reaches the 85% level only after 230 min of the reaction. The lower rate of the photocatalytic oxidation of substrates that deactivate TiO_2 photocatalyst at low air RH is in agreement with other authors [36] and our previous findings [23,24]. Over thin film TiO_2, the formation of CO_2 occurs at a 30% higher rate at RH 50% compared to RH 1%. The mentioned influence of the water vapor can be explained via the following simplified scheme of the DMMP removal and oxidation.

$$\mathrm{DMMP(g) + Z \rightleftarrows DMMP(ads)}, \quad \text{(I)}$$

$$\mathrm{DMMP(ads) + H_2O(ads) \rightarrow MMP(ads) + CH_3OH}, \quad \text{(II)}$$

$$\mathrm{TiO_2 + h\nu \rightleftarrows e^- + h^+} \quad \text{(III)}$$

$$\mathrm{O_2 + Z + e^- \rightarrow O_2^-(ads)}, \quad \text{(IV)}$$

$$\mathrm{MMP(ads) + h^+ \rightarrow \ldots + O_2^-(ads) \rightarrow H_3PO_4(ads) + 2CO_2(g)}, \quad \text{(V)}$$

$$\mathrm{H_2O\,(g) \rightleftarrows H_2O\,(ads)}, \quad \text{(VI)}$$

$$\mathrm{H_2O\,(g) \rightleftarrows H_2O\,(ads\ multilayer)} \quad \text{(VII)}$$

$$\mathrm{H_3PO_4\,(ads) + H_2O\,(ads\ multilayer) \rightleftarrows H_3PO_4\,(solv.\ multilayer) + Z} \quad \text{(VIII)}$$

In this scheme, Z is an unoccupied TiO_2 adsorption site, MMP is methyl methylphosphonic acid, (g) refers to gaseous and (ads) refers to adsorbed species.

The increase of the water vapor concentration increases the surface coverage of water (stages VI and VII) that competes with DMMP for the adsorption sites. A smaller coverage with DMMP results in a slower rate of the hydrolysis (stage II). However, multilayer of adsorbed water is able to dissolve phosphoric acid (stage VIII), which is the final product of the DMMP photocatalytic oxidation via the stage V. Phosphoric acid is known to deactivate TiO_2 in the gas phase DMMP photocatalytic oxidation [37] but has little influence in the liquid phase [38]. The released adsorption sites participate in photoadsorption of dioxygen (stage IV) that is important for separation of charges photogenerated in TiO_2 (stage III) and oxidation stages (V).

Note that the very fast air purification obtained in the photocatalyst aerosol system under the study agrees well with an estimate of characteristic time for the substrate molecule diffusion from the bulk to the aerosol particles. Indeed, the characteristic time τ of external diffusion can be estimated as

$$\tau = \frac{L^2}{6D}$$

where L is the characteristic mean diffusion length (cm), D is the diffusion coefficient ($cm^2\ s^{-1}$). If the aerosol concentration is N (cm^{-3}), then the characteristic external diffusion time is estimated as

$$\tau = \frac{1}{6DN^{2/3}}$$

Taking $D \sim 0.025\ cm^2\ s^{-1}$ for DMMP [24] this formula shows that the time of external diffusion is below 1 ms if the aerosol concentration is above $10^6\ cm^{-3}$. This is the case in our study. Thus, adsorption of the gas phase substrates takes place as soon as new portions of TiO_2 aerosol become available.

Table 5 summarizes the rates and quantum efficiencies of adsorptive-photocatalytic air purification observed in the present

Table 4
Parameters of the air purification from the DMMP vapors under UV radiation.

Figure number	Relative humidity (%)	Characteristic time of DMMP removal (min)		Consumption of DMMP (%)		Initial rate of the CO_2 formation (ppm/min)	Initial rate of the methanol generation (ppm/min)	Characteristic time of methanol removal (min)
		τ_1	τ_2	$2\tau_1$	$2\tau_2$			
Fig. 9	37 ± 3	0.6 ± 0.1	31 ± 21	85	~100	7.4	7.42	4.5 ± 0.3
Fig. 10	4 ± 1	0.3 ± 0.1	62 ± 55	87	~100	3.8	4.7	2.3 ± 0.2

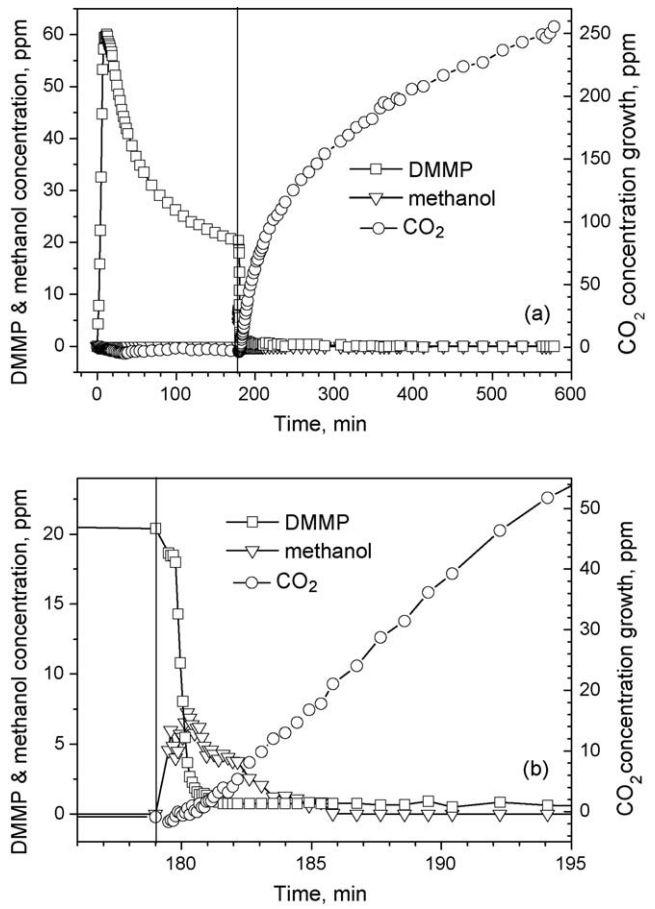

Fig. 10. (a) Temporal concentration profiles at the simultaneous adsorption and photocatalytic oxidation of DMMP under air humidity 4 ± 1%. t = 0 min corresponds to the injection of DMMP, t = 179 min (vertical line)—to the start of aerosol generation. (b) Magnified part of the plot corresponding to the fast adsorption and hydrolysis period.

Table 5
Summary of the rates and quantum efficiencies in the adsorptive-photocatalytic air purification over TiO_2 aerosol. The initial oxidation rates were calculated from the initial CO_2 formation rates (Tables 2 and 4). The initial overall quantum efficiencies were calculated with Eq. (2).

Substrate	Relative humidity (%)	Initial substrate removal rate (ppm/min)	Initial deep oxidation rate (nmol s^{-1})	Initial overall quantum efficiency of photocatalytic oxidation (%)
Acetone	37	23	300	39
Acetone	4	54	230	30
DMMP	37	16	170	28
DMMP	4	39	90	15

study. Acetone and DMMP vapors are initially removed by the TiO_2 aerosol very quickly and mineralized with a high overall quantum efficiency. The increase in the air relative humidity strongly decreases the initial rate of the adsorptive removal stage, but increases the rate and the initial overall quantum efficiency of photocatalytic mineralization. Since no more than ~40% of UV light emitted by the UV lamp is absorbed by the photocatalyst in the chamber, the quantum yields of photocatalytic oxidation can be twice or more higher than the quantum efficiencies listed in Table 5.

4. Conclusions

The major findings of this study are the following.

- Aerosol of TiO_2 particles with the average particles size ~0.5 μm and the concentration as high as 1.5×10^6 cm^{-3} was produced in the 0.1 m^3 experimental chamber using the sonic generator operated for 10 min.
- The rate of air purification from acetone and the DMMP vapor by the TiO_2 aerosol particles is limited by the rate of the aerosol generation and depends on adsorption and reaction constants. For the case of the low substrate adsorption constant (acetone at RH 37%), the UVA irradiation accelerates significantly the purification rate, while for the cases of high substrate adsorption constant (DMMP) the substrate removal is not accelerated by the irradiation.
- Acetone adsorbs reversibly over the TiO_2 aerosol, the adsorption equilibration time being below 0.5 min. The Langmuir isotherm model fits well to the concentration vs. aerosol mass dependence and allows obtaining the values of the adsorption constant and monolayer coverage for air relative humidity 4 and 37% (296 K).
- The adsorption of DMMP over the TiO_2 aerosol particles surface initiates the DMMP hydrolysis with the formation of gaseous methanol and non-volatile methyl methylphosphonate in the timescale below 10 s. Irreversible character of this DMMP adsorption makes air purification from DMMP vapor a fast process with the characteristic time 20–40 s.
- The increase of the air relative humidity decreases adsorption rate and extent of acetone and DMMP while increases significantly the rate of the acetone and DMMP photocatalytic oxidation.
- Photocatalytic oxidation turned out to be indispensable for the complete air purification from organic compounds by the TiO_2 aerosol since the adsorption alone did not remove acetone and toxic DMMP hydrolysis product methanol from the gas phase completely.

Acknowledgements

We gratefully acknowledge the partial support for this research by ISTC via project 3305, NATO via project SfP-981461, RAS Presidium project 27.56 and Integration projects 36 and 70. Help of Dr. Kozlov in development of IR data processing methods is greatly appreciated.

References

[1] V.N. Filimonov, Dokl. Akad. Nauk. 158 (1964) 1408–1411.
[2] I.S. McLintock, M. Ritchie, Trans. Faraday Soc. 61 (1965) 1007–1016.
[3] L.V. Lyashenko, Ya.B. Gorokhovatsky, Theor. Exp. Chim. 10 (1974) 186–192.
[4] N. Djeghri, M. Formenti, F. Juillet, S.J. Teichner, Faraday Disc. Chem. Soc. 58 (1974) 185–193.
[5] O. Carp, C.L. Huisman, A. Reller, Prog. Solid State Chem. 32 (2004) 33–177.
[6] K. Onoda, S. Yoshikawa, Appl. Catal. B 80 (2008) 277–285.
[7] I.A. Baturov, A.V. Vorontsov, D.V. Kozlov, Russ. Chem. Bull. 54 (2005) 1866–1873.
[8] T. Guo, Z. Bai, C. Wu, T. Zhu, Appl. Catal. B 79 (2008) 171–178.
[9] S. Matsuda, H. Hatano, A. Tsutsumi, Chem. Eng. J. 82 (2001) 183–188.
[10] K.-P. Yu, G.W.M. Lee, Appl. Catal. B 75 (2007) 29–38.
[11] L.A. Dibble, G.B. Raup, Environ. Sci. Technol. 26 (1992) 492–495.
[12] T.H. Lim, S.D. Kim, Chemosphere 54 (2004) 305–312.
[13] M. Nazir, J. Takasaki, H. Kumazawa, Chem. Eng. Commun. 190 (2003) 322–333.
[14] T.H. Lim, S.D. Kim, Chem. Eng. Process 44 (2005) 327–334.
[15] A.V. Vorontsov, E.N. Savinov, P.G. Smirniotis, Chem. Eng. Sci. 55 (2000) 5089–5098.
[16] O. Prieto, J. Fermoso, R. Irusta, Int. J. Photoenergy (2007) 32859.
[17] M. Lim, V. Rudolph, M. Anpo, G.Q. Lu, Catal. Today 131 (2008) 548–552.
[18] T.H. Lim, S.M. Jeong, S.D. Kim, J. Gyenis, J. Photochem. Photobiol. A 134 (2000) 209–217.
[19] K.I. Zamaraev, M.I. Khramov, V.N. Parmon, Catal. Rev.-Sci. Eng. 36 (1994) 617–644.
[20] V.N. Parmon, V.S. Zakharenko, CatTech. 5 (2001) 96–115.
[21] V.N. Parmon, K.I. Zamaraev, in: G. Ertl, H. Knozinger, J. Weitkamp (Eds.), Handbook of Heterogeneous Catalysis, vol. 4, 1997, pp. 1686–1695.
[22] C.N. Rusu, J.T. Yates, J. Phys. Chem. B 104 (2000) 12299–12305.
[23] D.A. Trubitsyn, A.V. Vorontsov, Mendeleev Commun. 5 (2004) 197–199.
[24] D.A. Trubitsyn, A.V. Vorontsov, J. Phys. Chem. B 109 (2005) 21884–21892.
[25] A. Kiselev, A. Mattson, M. Andersson, A.E.C. Palmqvist, L. Osterlund, J. Photochem. Photobiol. A 184 (2006) 125–134.

[26] A.V. Vorontsov, C. Lion, E.N. Savinov, P.G. Smirniotis, J. Catal. 220 (2003) 414–423.
[27] V.H. Grassian, A. Adamcakova-Dodd, J.M. Pettibone, P.T. O'Shaughnessy, P.S. Thorne, Nanotoxicology 1 (2007) 211–226.
[28] A.S. Besov, A.V. Vorontsov, Catal. Commun 9 (2008) 2598–2600.
[29] S.E. Braslavsky, Pure Appl. Chem. 79 (2007) 293–465.
[30] A.V. Vorontsov, I.V. Stoyanova, D.V. Kozlov, V.I. Simagina, E.N. Savinov, J. Catal. 189 (2000) 360–369.
[31] A.L. McClellan, H.F. Harnsberger, J. Colloid. Interface Sci. 23 (1967) 577.
[32] M. El-Maazawi, A.N. Finken, A.B. Nair, V.H. Grassian, J. Catal. 191 (2000) 138–146.
[33] M.A. Henderson, J. Phys. Chem. B 109 (2005) 12062–12070.
[34] A.V. Vorontsov, E.N. Savinov, Chem. Eng. J. 70 (1998) 231–235.
[35] M.L. Sauer, D.F. Ollis, J. Catal. 149 (1994) 81–91.
[36] T. Guo, Z.P. Bai, C. Wu, T. Zhu, Appl. Catal. B 79 (2008) 171–178.
[37] T.N. Obee, S. Satyapal, J. Photochem. Photobiol. A: Chem. 118 (1998) 45–51.
[38] P. Raja, V. Nadtochenko, U. Klehm, J. Kiwi, Appl. Catal. B 81 (2008) 258–266.